

Spin-orbit Coupled Bose-Einstein Condensates in Spin-dependent Optical Lattices

Wei Han,^{1,2} Suying Zhang,² and Wu-Ming Liu¹

¹Beijing National Laboratory for Condensed Matter Physics,

Institute of Physics, Chinese Academy of Sciences, Beijing 100190, China

²Institute of Theoretical Physics, Shanxi University, Taiyuan 030006, China

We investigate the ground-state properties of spin-orbit coupled Bose-Einstein condensates in spin-dependent optical lattices. The competition between the spin-orbit coupling strength and the depth of the optical lattice leads to a rich phase diagram. Without spin-orbit coupling, the spin-dependent optical lattices separate the condensates into alternating spin domains with opposite magnetization directions. With relatively weak spin-orbit coupling, the spin domain wall is dramatically changed from Néel wall to Bloch wall. For sufficiently strong spin-orbit coupling, vortex chains and antivortex chains are excited in the spin-up and spin-down domains respectively, corresponding to the formation of a lattice composed of meron-pairs and antimeron-pairs in the pseudospin representation. We also discuss how to observe these phenomena in real experiments.

PACS numbers: 03.75.Lm, 03.75.Mn, 05.30.Jp, 67.85.Fg

Introduction.—In recent years, the experimental control on ultracold atomic gases has reached truly unprecedented levels. By employing two lasers with different frequencies and polarizations plus a non-uniform vertical magnetic field, experimentalists have produced spin-orbit (SO) coupling, which couples the internal states and the orbit motion of the atoms [1–4]. The SO coupled ultracold atomic gases have attracted great interests of researchers [5–15]. It has been indicated that the interplay among SO coupling, interatomic interaction and external potential leads to rich ground-state phases, such as plane wave, density stripe, fractional vortex and various vortex lattices [16–26]. The SO coupled ultracold atomic gases open a new window for quantum simulation, and provide opportunities to study SO coupling phenomena in a highly controllable impurity-free environment.

All the existing studies on SO coupled Bose-Einstein condensates (BECs) only refer to the case that different internal states of the atoms are trapped in an identical external potential. However, by using two counterpropagating lasers with the same frequency but different polarizations, the experimentalists have been able to produce spin-dependent optical lattices that allow different internal states of the atoms experience drastically different external potentials [27–31]. The spin-dependent optical lattices bring more complicated geometry of condensates and have potential applications in quantum computation [27], cooling and thermometry [28], and quantum simulation [29–32]. It is natural to ask what new structures can be formed due to the competition between the SO coupling and the spin-dependent optical lattices.

In this Letter, we investigate the ground-state phase diagram of SO coupled BECs in spin-dependent optical lattices. In the absence of SO coupling, the ground state of the system is characterized by the formation of alternating spin domains. However, such a structure can be dramatically changed due to the SO coupling effects. Relatively weak SO coupling basically changes the ori-

entation of the spins in the domain walls, causing the transformation from Néel wall to Bloch wall. Sufficiently strong SO coupling excites meron-pairs and antimeron-pairs in the spin-up and spin-down domains respectively and generates a meron-pair lattice. This is essentially different from the mechanism of generating a meron-pair lattice by bulk rotation [33]. Our findings provide a new way to create and manipulate topological excitations in SO coupled systems.

Energy band structure.—We consider SO coupled BECs confined in the combined potential of a quasi-2D harmonic trap and 1D spin-dependent optical lattices. The Hamiltonian of this system is given by

$$\mathcal{H} = \int d\mathbf{r} \left[\Psi^\dagger \left(-\frac{\hbar^2 \nabla^2}{2m} + \mathcal{V}_{\text{so}} \right) \Psi + V_1(\mathbf{r})n_\uparrow + V_2(\mathbf{r})n_\downarrow + g_{11}n_\uparrow^2 + g_{22}n_\downarrow^2 + g_{12}n_\uparrow n_\downarrow \right], \quad (1)$$

where $\Psi = [\Psi_\uparrow(\mathbf{r}), \Psi_\downarrow(\mathbf{r})]^T$ denotes the two-component wave functions and is normalized as $\int d\mathbf{r} \Psi^\dagger \Psi = N$ with

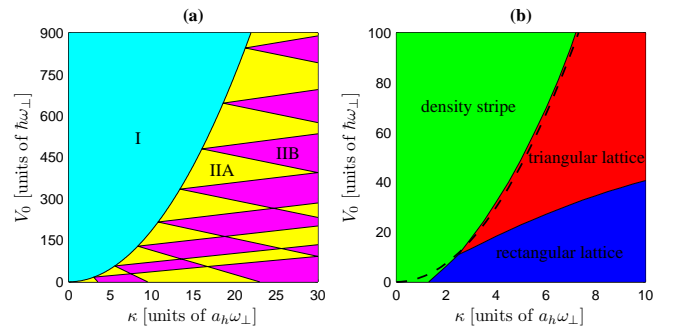


FIG. 1: (Color online) (a) Single-particle phase diagram spanned by the SO coupling strength κ and the depth V_0 of the optical lattice. (b) Many-body phase diagram spanned by κ and V_0 with the effective interaction parameter $\tilde{g} = 6000$. The dashed line in (b) indicates the phase boundary between phase I and phase II in (a) for comparison.

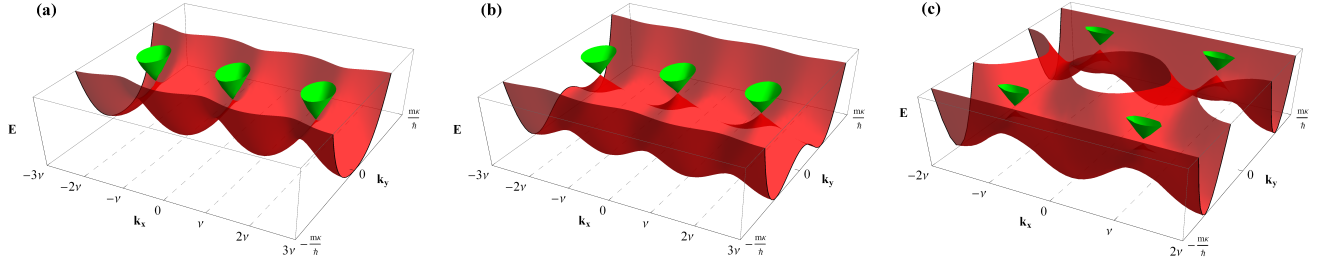


FIG. 2: (Color online) Band structures induced by the competition between the SO coupling strength κ and the depth V_0 of the optical lattice corresponding to phase I (a), phase IIA (b), and phase IIB (c) of the single-particle phase diagram in Fig. 1(a). The superposition of the momenta at the minima of the bands produces a density stripe in (a), a lattice in (b) and (c).

N the total particle number. $n_\uparrow = \Psi_\uparrow^* \Psi_\uparrow$ and $n_\downarrow = \Psi_\downarrow^* \Psi_\downarrow$ describe the particle number density of each component. $g_{ij} = 4\pi\hbar^2 a_{ij}/m$ ($i, j = 1, 2$) represent the interatomic interaction strengths characterized by the s -wave scattering lengths a_{ij} and the atomic mass m .

We consider a Rashba SO coupling $\mathcal{V}_{\text{so}} = -i\hbar\kappa(\sigma_x\partial_x + \sigma_y\partial_y)$, where $\sigma_{x,y}$ are the Pauli matrices and κ denotes the SO coupling strength. The combined external potential $V_i(\mathbf{r}) = V_H(\mathbf{r}) + V_{\text{OL}i}(x)$, where $V_H = \frac{1}{2}m\omega_\perp^2[(x^2 + y^2) + \lambda^2 z^2]$ is the harmonic trapping potential with $\lambda = \omega_z/\omega_\perp \gg 1$, and $V_{\text{OL}1} = V_0 \sin^2(\nu x)$ and $V_{\text{OL}2} = V_0 \cos^2(\nu x)$ describe the 1D spin-dependent optical lattice potentials, which are experienced by the two components, respectively. Approximating the z dependence of the wave functions by the single-particle ground state in a harmonic potential, one can obtain the 2D dimensionless effective interaction parameters $\tilde{g}_{ij} = 2\sqrt{2}\pi\lambda N a_{ij}/a_h$, with $a_h = \sqrt{\hbar/(m\omega_\perp)}$ [34].

The single-particle energy bands are critically important to understand the ground-state properties of the condensates. Without considering the harmonic trap, the 2D single-particle wave functions in the k -space obey the secular equations $\frac{\hbar^2}{2m}[(k_x + 2s\nu)^2 + k_y^2]U_s - \frac{V_0}{4}(U_{s+1} - 2U_s + U_{s-1}) + \hbar\kappa(k_x + 2s\nu - ik_y)W_s = \varepsilon U_s$ and $\frac{\hbar^2}{2m}[(k_x + 2s\nu)^2 + k_y^2]W_s + \frac{V_0}{4}(W_{s+1} + 2W_s + W_{s-1}) + \hbar\kappa(k_x + 2s\nu + ik_y)U_s = \varepsilon W_s$, where $U_s = U(k_x + 2s\nu, k_y)$ and $W_s = W(k_x + 2s\nu, k_y)$ with $s = 0, \pm 1, \pm 2, \dots, \pm\infty$ represent the wave functions at the point $(k_x + 2s\nu, k_y)$. Typically, we choose $\nu = a_h^{-1}$ for our present discussion. By numerical exact diagonalization, we can solve the secular equations and obtain the energy band structure.

We find that there exist three different kinds of energy band structures depending on the competition between the SO coupling strength κ and the depth V_0 of the optical lattices. Fig. 1(a) presents the single-particle phase diagram spanned by κ and V_0 . In phase I, the minima of the energy bands locate in a set of k points with $k_y = 0$ and $k_x \in K_1 = \{\pm\nu, \pm 3\nu, \pm 5\nu, \dots\}$ [See Fig. 2(a)]. In phase II, the minima of the energy bands locate in a set of k points with $k_y = \pm\delta$ ($0 < \delta \leq \frac{m\kappa}{\hbar}$), and $k_x \in K_1$ for phase IIA ($k_x \in K_2 = \{0, \pm 2\nu, \pm 4\nu, \pm 6\nu, \dots\}$ for phase

IIB) [See Figs. 2(b) and 2(c)].

The single-particle ground state in phase I is nondegenerate and can be expressed as a linear superposition of the plane waves with wave vectors $(k_x \in K_1, k_y = 0)$. This yields alternating spin domains with opposite magnetization directions (density stripe). In both phase IIA and phase IIB, the single-particle ground state is double-degenerate. Each degenerate state can be expressed as a linear superposition of the plane waves with wave vectors $(k_x \in K, k_y = \delta)$ or $(k_x \in K, k_y = -\delta)$, where $K = K_1$ for phase IIA and $K = K_2$ for phase IIB. For an arbitrary nonzero superposition of the two degenerate states, lattice will be formed as the single-particle ground state.

Phase diagram.—By using the imaginary time evolution method, we can solve Eq. (1) to obtain the many-body ground state. Considering that the spin-exchange integrations are very weak in typical experiments, we just discuss the case that $\tilde{g}_{ij} = \tilde{g}$. The many-body phase diagram spanned by κ and V_0 with $\tilde{g} = 6000$ is presented in Fig. 1(b). We find that the competition between the SO coupling strength and the depth of the optical lattice leads to three distinct phases—density stripe, triangular vortex lattice and rectangular vortex lattice.

In the density stripe phase, the spin-up and spin-down components are arranged alternately and form alternating spin domains [See Figs. 3(a1-a6)]. Comparing the phase diagrams in Figs. 1(a) and 1(b), we find that the interaction has no significant influence on the phase region of the density stripe.

In the vortex lattice phases, both the triangular and rectangular lattices are composed of alternately arranged vortex and antivortex chains, which are excited in the spin-up and spin-down domains respectively [See Figs. 3(b1-b6) and 3(c1-c6)]. The only difference is that the vortices of the neighboring chains are staggered for the triangular lattice, but are parallel for the rectangular lattice [See Figs. 3(b3) and 3(c3)]. These two different arrangements of vortices correspond to odd-parity and even-parity distributions of the particles in k_x direction of the k -space. [See Figs. 3(b6) and 3(c6)]. These correspond to the single particle band structures described in Figs. 2(c) and (b), where the minima of

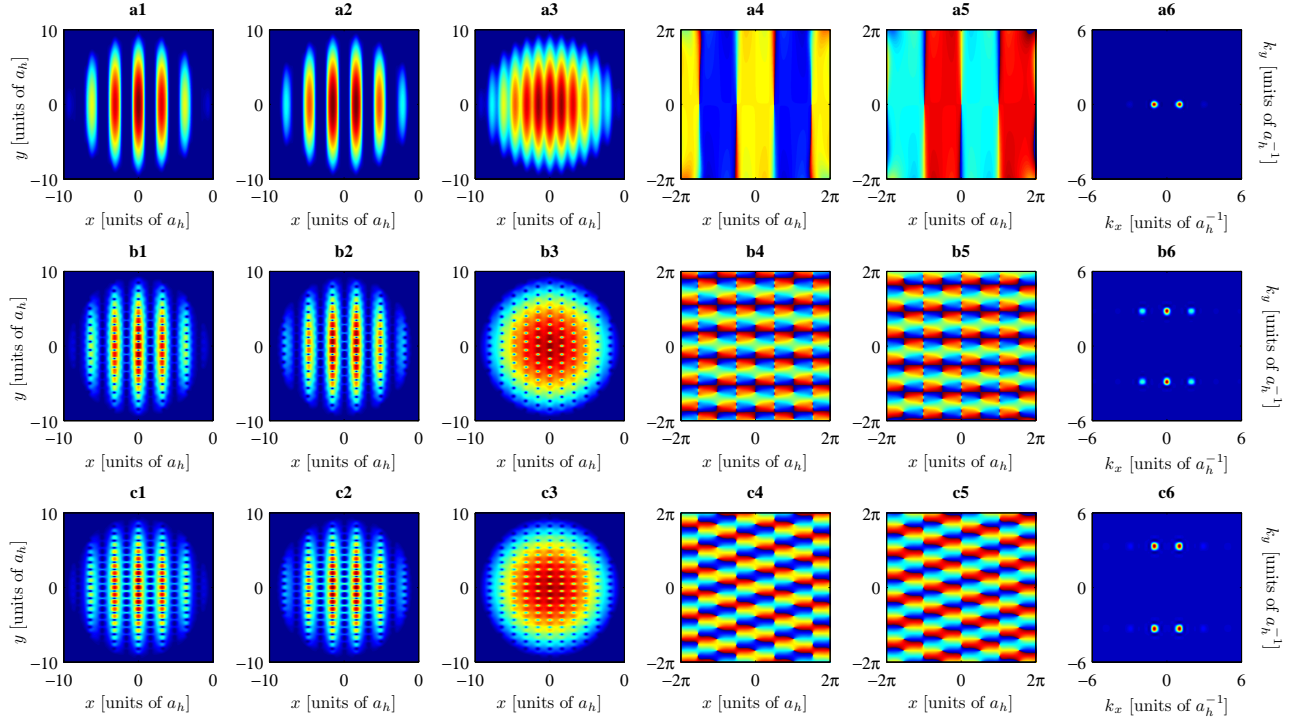


FIG. 3: (Color online) Ground state as a function of the SO coupling strength κ and the depth V_0 of the optical lattice with $\kappa = 4a_h\omega_\perp$, $V_0 = 40\hbar\omega_\perp$ (a1-a6), $\kappa = 4a_h\omega_\perp$, $V_0 = 20\hbar\omega_\perp$ (b1-b6), $\kappa = 4a_h\omega_\perp$, $V_0 = 15\hbar\omega_\perp$ (c1-c6). The effective interaction parameter is fixed at $\tilde{g} = 6000$. The spin-up, spin-down, and total density profiles are shown in (a1, b1, c1), (a2, b2, c2), and (a3, b3, c3), respectively. The phases of the spin-up and spin-down wave functions, with values ranging from $-\pi$ to π (blue to red), are shown in (a4, b4, c4) and (a5, b5, c5). The momentum distributions are depicted in (a6, b6, c6).

the bands also show odd-parity and even-parity distributions respectively, although their phase regions are not consistent due to the influence of the interatomic interactions [See Figs. 1(a) and 1(b)]. As discussed above, the single-particle ground state in phase II is double-degenerate. From Figs. 3(b6) and 3(c6), we can see that the interaction removes the degeneracy and chooses an equal weighted linear superposition of the two degenerate states as the many-body ground state.

The alternating arrangement of the vortex and antivortex chains leads to alternating-direction plane waves, which propagating on two sides of each chain [See Figs. 3(b4,b5) and 3(c4,c5)]. The vortex line density n_v and the wave number of the plane waves k_y satisfy $n_v = \frac{k_y}{\pi}$. Numerical simulations indicate that for a given SO coupling strength κ , as the lattice depth V_0 increases from 0, k_y gradually decreases from $\frac{m\kappa}{\hbar}$ and eventually becomes 0 on the boundary of the vortex lattice phase. This implies that by adjusting the depth of the optical lattice, one can continuously control the vortex line density from 0 to $\frac{m\kappa}{\pi\hbar}$.

Spin domain wall.—The separation between the spin-up and spin-down domains is not sharp, but requires the spin density vector varying gradually across the opposite domains and forming a spin domain wall [35]. There are two basic types of domain walls, Néel wall and Bloch

wall. In the Néel wall spin flip occurs in a plane, while in the Bloch wall the spin flip occurs by tracing a helix [See Figs. 4(b1) and 4(b2)]. An intriguing finding of the present work is that the SO coupling dramatically changed the domain wall from Néel wall to Bloch wall. Figs. 4(a1) and 4(a2) show the spin density vector $\mathbf{S} = \frac{\Psi^\dagger \boldsymbol{\sigma} \Psi}{|\Psi|^2}$ without and with SO coupling. We can see that in the absence of SO coupling, the spin density vector across the opposite domains forms a Néel wall, while in the presence of SO coupling it forms a Bloch wall.

This phenomenon can be understood as follows. The direction of the spin flip in the domain wall only depends on the relative phase, and can be represented by an azimuthal angle $\alpha = \arctan(S_y/S_x) = \theta_\downarrow - \theta_\uparrow$, where θ_\uparrow and θ_\downarrow are the phases of the wave functions. When the SO coupling is absent, there is a constant phase difference 0 or π [See the solid line of Fig. 4(c)], so the spin in the walls just flips along the x -direction and forms Néel walls. When the SO coupling is present, the phase difference is changed into $\pm \frac{\pi}{2}$ [See the dashed line of Fig. 4(c)], so the spin in the walls just flips along the y -direction and forms Bloch walls.

Meron-pair lattice.—The regular triangular or rectangular vortex lattice obtained in Fig. 3 can be equivalently described by the spin density vector \mathbf{S} in the pseudospin representation. Fig. 5(a) presents the vectorial plots of \mathbf{S}

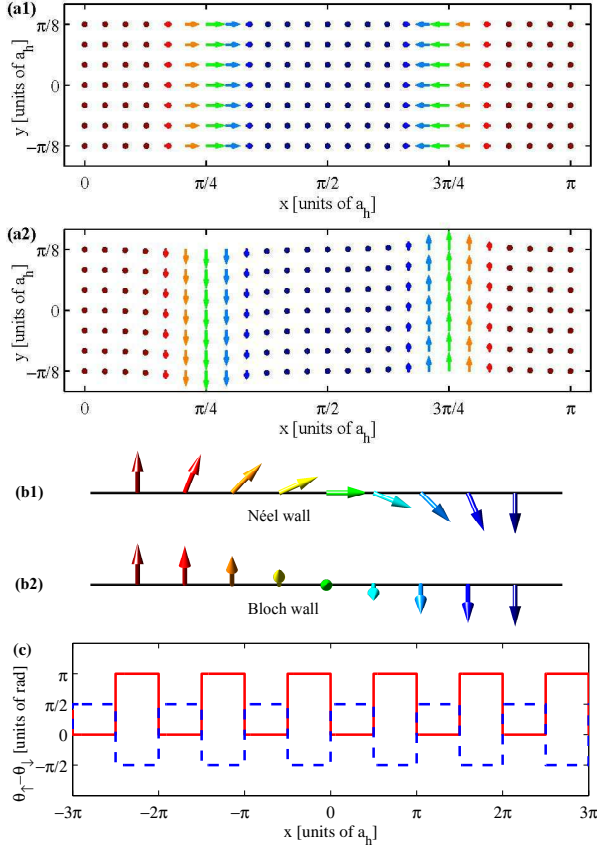


FIG. 4: (Color online) (a) The vectorial plots of the pseudospin \mathbf{S} projected onto the x - y plane with $\tilde{g} = 6000$, $V_0 = 40\hbar\omega_\perp$, and $\kappa = 0$ (a1), $\kappa = 4a_h\omega_\perp$ (a2). The colors ranging from blue to red describe the values of the axial spin S_z from -1 to 1 . (b) 3D renderings of Néel wall and Bloch wall. (c) Section views of the relative phase $\theta_+ - \theta_-$ along the x axis with $\kappa = 0$ (solid line) and $\kappa = 4a_h\omega_\perp$ (dashed line).

under a pseudo-spin rotation, which corresponding to the state represented in Figs. 3(c1-c6), and the corresponding topological charge density $q(\mathbf{r}) = \frac{1}{8\pi}\epsilon^{ij}\mathbf{S} \cdot \partial_i\mathbf{S} \times \partial_j\mathbf{S}$ is plotted in Fig. 5(b). One can see that the spin texture in Fig. 5(a) represents a lattice composed of meron pairs and antimeron pairs [36, 37]. Either a meron pair or an antimeron pair has a “circular-hyperbolic” structure [See Figs. 5(c1) and 5(c2)], and the only difference is that they have exactly opposite spin orientations. The spatial integral of $q(\mathbf{r})$ indicates that a meron pair just carries topological charge 1, while an antimeron pair carries topological charge -1 . Previous studies indicated that stable meron-pair lattice can be obtained in a rotating system [33]. Our results show that meron-pair lattice can also be stabilized in alternating spin domains by SO coupling without rotation.

Experimental proposal.—In real experiments, we can choose a two-level ^{87}Rb BEC system with $|F=1, m_f=1\rangle$ and $|F=1, m_f=-1\rangle$. About $N = 1.7 \times 10^5$ atoms are confined in a harmonic trap with the

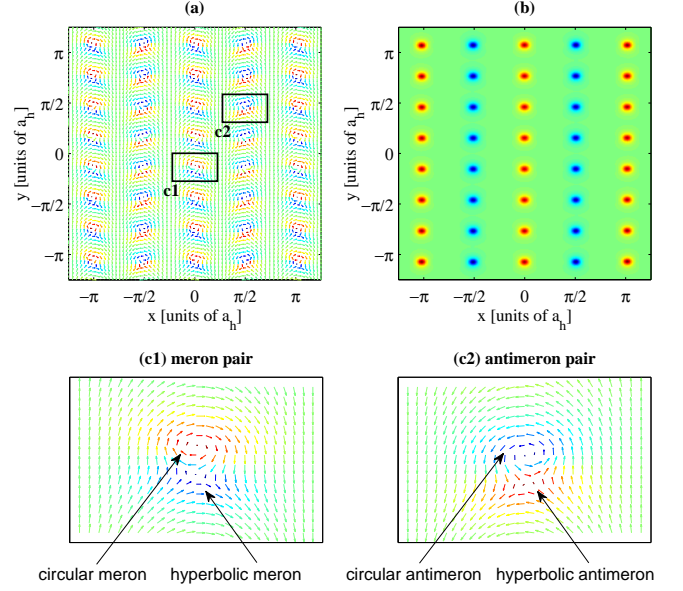


FIG. 5: (Color online) (a) The vectorial plots of the pseudospin \mathbf{S} projected onto the x - y plane under a pseudo-spin rotation $\sigma_x \rightarrow -\sigma_z$ and $\sigma_z \rightarrow \sigma_x$. (b) The topological charge density $q(\mathbf{r})$. (c) The amplification of the two kinds of elements in (a).

trapping frequencies $\omega_\perp \approx 2\pi \times 40$ Hz and $\omega_z \approx 2\pi \times 200$ Hz. It is convenient to produce spin-dependent optical lattices with a large lattice spacing by using a CO_2 laser operated at a wavelength of $10.6 \mu\text{m}$. Under typical experimental conditions, the s -wave scattering lengths $a_{ij} \approx 100a_B$ (a_B is the Bohr radius). Based on these experimental parameters, we can calculate that the effective interaction parameter $\tilde{g} \approx 6000$ and the wave vector $\nu = a_h^{-1}$, which are consistent with our present calculation.

For a given SO coupling strength $\kappa = 4\sqrt{\hbar\omega_\perp/m}$, adjusting the lattice depth from $V_0 = k_B \times 80$ nK to $V_0 = k_B \times 40$ nK, then to $V_0 = k_B \times 30$ nK (k_B is the Boltzmann’s constant), one can directly observe the phase transitions from density stripe to triangular vortex lattice, then to rectangle vortex lattice by monitoring in situ the density profile. And for a given lattice depth $V_0 = k_B \times 80$ nK, adjusting the SO coupling strength from $\kappa = 0$ to $\kappa = 4\sqrt{\hbar\omega_\perp/m}$, one may indirectly observe the transition of the spin domain wall from Néel wall to Bloch wall by dual state imaging technique, which can spatially resolve the relative phase [38].

Conclusion.—In summary, we have investigated the ground-state phase diagram of spin-orbit coupled BECs in spin-dependent optical lattices. We observe novel spin-orbit coupling effects on alternating spin domains produced by the spin-dependent optical lattices. Actually, alternating spin domains exist in many physical systems, such as magnetic materials and condensed matter systems [39, 40], thus similar spin-orbit coupling effects

would be discovered in those systems. We hope that our findings will deepen the understanding of spin-orbit coupling phenomena and provide thoughts on engineering new quantum states in spin-orbit coupled systems.

We are grateful to Shih-Chuan Gou for helpful discussions. This work was supported by the NKBRSCF under Grants No. 2011CB921502, No. 2012CB821305, No. 2009CB930701, and No. 2010CB922904, NSFC under Grants No. 10972125 and No. 10934010, NSFC-RGC under Grants No. 11061160490 and No. 1386-N-HKU748/10, NSFSP under Grant No. 2010011001-2, and SFRSP.

-
- [1] Y. J. Lin, K. Jiménez-García, and I. B. Spielman, *Nature* (London) **471**, 83 (2011).
 - [2] P. Wang, Z. Q. Yu, Z. Fu, J. Miao, L. Huang, S. Chai, H. Zhai, and J. Zhang, *Phys. Rev. Lett.* **109**, 095301 (2012).
 - [3] L. W. Cheuk, A. T. Sommer, Z. Hadzibabic, T. Yefsah, W. S. Bakr, and M. W. Zwierlein, *Phys. Rev. Lett.* **109**, 095302 (2012).
 - [4] J. Y. Zhang, S. C. Ji, Z. Chen, L. Zhang, Z. D. Du, B. Yan, G. S. Pan, B. Zhao, Y. J. Deng, H. Zhai, S. Chen, and J. W. Pan, *Phys. Rev. Lett.* **109**, 115301 (2012).
 - [5] J. Dalibard, F. Gerbier, G. Juzeliūnas, and P. Öhberg, *Rev. Mod. Phys.* **83**, 1523 (2011).
 - [6] A. M. Dudarev, R. B. Diener, I. Carusotto, and Q. Niu, *Phys. Rev. Lett.* **92**, 153005 (2004).
 - [7] T. D. Stanescu, B. Anderson, and V. Galitski, *Phys. Rev. A* **78**, 023616 (2008).
 - [8] X. F. Zhou, J. Zhou, and C. Wu, *Phys. Rev. A* **84**, 063624 (2011).
 - [9] Z. Cai, X. Zhou, and C. Wu, *Phys. Rev. A* **85**, 061605(R) (2012).
 - [10] X. Q. Xu and J. H. Han, *Phys. Rev. Lett.* **107**, 200401 (2011).
 - [11] R. Liao, Y. Yi-Xiang, and W. M. Liu, *Phys. Rev. Lett.* **108**, 080406 (2012).
 - [12] Y. Li, L. P. Pitaevskii, and S. Stringari, *Phys. Rev. Lett.* **108**, 225301 (2012).
 - [13] T. Ozawa and G. Baym, *Phys. Rev. Lett.* **109**, 025301 (2012).
 - [14] W. S. Cole, S. Zhang, A. Paramekanti, and N. Trivedi, *Phys. Rev. Lett.* **109**, 085302 (2012).
 - [15] J. Radić, A. Di Ciolo, K. Sun, and V. Galitski, *Phys. Rev. Lett.* **109**, 085303 (2012).
 - [16] C. Wang, C. Gao, C. M. Jian, and H. Zhai, *Phys. Rev. Lett.* **105**, 160403 (2010).
 - [17] T. L. Ho and S. Zhang, *Phys. Rev. Lett.* **107**, 150403 (2011).
 - [18] Z. F. Xu, R. Lü, and L. You, *Phys. Rev. A* **83**, 053602 (2011).
 - [19] S. Sinha, R. Nath, and L. Santos, *Phys. Rev. Lett.* **107**, 270401 (2011).
 - [20] Y. Zhang, L. Mao, and C. Zhang, *Phys. Rev. Lett.* **108**, 035302 (2012).
 - [21] H. Hu, B. Ramachandhran, H. Pu, and X. J. Liu, *Phys. Rev. Lett.* **108**, 010402 (2012).
 - [22] B. Ramachandhran, B. Opanchuk, X. J. Liu, H. Pu, P. D. Drummond, and H. Hu, *Phys. Rev. A* **85**, 023606 (2012).
 - [23] Y. Deng, J. Cheng, H. Jing, C. P. Sun, and S. Yi, *Phys. Rev. Lett.* **108**, 125301 (2012).
 - [24] S. W. Su, I. K. Liu, Y. C. Tsai, W. M. Liu, and S. C. Gou, *Phys. Rev. A* **86**, 023601 (2012).
 - [25] Z. F. Xu, Y. Kawaguchi, L. You, and M. Ueda, *Phys. Rev. A* **86**, 033628 (2012).
 - [26] E. Ruokokoski, J. A. M. Huhtamäki, and M. Möttönen, *Phys. Rev. A* **86**, 051607(R) (2012).
 - [27] O. Mandel, M. Greiner, A. Widera, T. Rom, T. W. Hänsch, and I. Bloch, *Phys. Rev. Lett.* **91**, 010407 (2003); *Nature* (London) **425**, 937 (2003).
 - [28] D. McKay and B. DeMarco, *New J. Phys.* **12**, 055013 (2010).
 - [29] C. Becker, P. Soltan-Panahi, J. Kronjäger, S. Dörscher, K. Bongs and K. Sengstock, *New J. Phys.* **12**, 065025 (2010).
 - [30] P. Soltan-Panahi, J. Struck, P. Hauke, A. Bick, W. Plenkers, G. Meineke, C. Becker, P. Windpassinger, M. Lewenstein, and K. Sengstock, *Nature Phys.* **7**, 434 (2011).
 - [31] P. Soltan-Panahi, D. Lühmann, J. Struck, P. Windpassinger, and K. Sengstock, *Nature Phys.* **8**, 71 (2012).
 - [32] P. Hauke, O. Tieleman, A. Celi, C. Ölschläger, J. Simonet, J. Struck, M. Weinberg, P. Windpassinger, K. Sengstock, M. Lewenstein, and A. Eckardt, *Phys. Rev. Lett.* **109**, 145301 (2012).
 - [33] K. Kasamatsu, M. Tsubota, and M. Ueda, *Phys. Rev. Lett.* **93**, 250406 (2004).
 - [34] K. Kasamatsu, M. Tsubota, and M. Ueda, *Phys. Rev. A* **67**, 033610 (2003).
 - [35] B. A. Malomed, H. E. Nistazakis, D. J. Frantzeskakis, and P. G. Kevrekidis, *Phys. Rev. A* **70**, 043616 (2004).
 - [36] G. E. Volovik, *The Universe in a Helium Droplet* (Oxford University, New York, 2003).
 - [37] F. Zhou, *Phys. Rev. B* **70**, 125321 (2004).
 - [38] R. P. Anderson, C. Ticknor, A. I. Sidorov, and B. V. Hall, *Phys. Rev. A* **80**, 023603 (2009).
 - [39] B. Vodungbo, J. Gautier, G. Lambert, A. B. Sardinha, M. Lozano, S. Sebhan, M. Ducouso, W. Boutu, K. Li, B. Tudu, M. Tortarolo, R. Hawaldar, R. Delaunay, V. López-Flores, J. Arabski, C. Boeglin, H. Merdji, P. Zeitoun, and J. Lüning, *Nature Commun.* **3**, 999 (2012).
 - [40] S. Erdin, I. F. Lyuksyutov, V. L. Pokrovsky, and V. M. Vinokur, *Phys. Rev. Lett.* **88**, 017001 (2001).